# Customized hybrid and NIR-light triggered thermoresponsive drug delivery microparticles synthetized by photopolymerization in a one-step flow focusing continuous microreactor

*Isabel Ortiz de Solorzano[†‡§*], Gracia Mendoza[†‡], Manuel Arruebo[†‡§*], Victor Sebastian[†‡§]*

[†]Department of Chemical Engineering. Aragon Institute of Nanoscience (INA) and Instituto de Ciencia de Materiales de Aragón (ICMA), Universidad de Zaragoza-CSIC, University of Zaragoza, Campus Río Ebro-Edificio I+D, C/ Poeta Mariano Esquillor S/N, 50018-Zaragoza, Spain

[‡]Aragon Health Research Institute (IIS Aragón), 50009 Zaragoza, Spain

[§]Networking Research Center on Bioengineering, Biomaterials and Nanomedicine, CIBER-BBN, 28029-Madrid, Spain

*Corresponding author: isaortiz@unizar.es; arruebom@unizar.es.

**KEYWORDS:** Thermoresponsive; photopolymerization; bupivacaine; microparticles; LED; microfluidics; coaxial; PNIPAm, Hollow gold nanoparticles, NIR-light triggered, drug delivery.

**ABSTRACT**

Photopolymerization is a selective technique that takes advantage of light-sensitive molecules to initiate and propagate monomeric structures to render covalently bonded macromolecular materials known as polymers. Herein, we present a novel one-step microfluidic synthesis of customized hybrid-thermoresponsive Poly(N-isopropylacrylamide) (PNIPAm) based microparticles (MPs) containing plasmonic hollow gold nanoparticles (HGNPs) and bupivacaine (BVP) used as a model drug. Those hybrid microparticles were prepared using a flow-focusing microreactor coupled to a UV LED device built with a simple outer PTFE tubing and an inner flexible capillary. Different tubing characteristics and flow rate ratios were altered in order to control the size of the resulting microparticles. In addition, components such as monomer, crosslinker and photoinitiator concentrations, as well as LED intensity and irradiation time were tuned to obtain different MPs and their characteristics and polymerization rates were compared by Gel permeation Chromatography (GPC). Thermoresponsive properties were analyzed and the presence of HGNPs was confirmed in light-activated triggered drug release applications. Bupivacaine loading and release studies were demonstrated with the resulting hollow and solid microparticles (which were obtained depending on the polymerization rate used) and their temperature responsiveness was assessed using a NIR laser when HGNPs were present in the constructs. Finally, cytotoxicity studies, cell-cycle arrest and apoptotic induction were carried out to certify their suitability for further biomedical applications to be used as triggerable drug depots.

# 1 Introduction

Engineered polymeric microparticles (MPs) have become very interesting multifunctional platforms in biomedicine.[1] Biosensing[2], drug delivery[3] or tissue engineering[4] are some of the areas in which MPs standout as advanced materials at the cutting edge of functional polymers. However, their biological suitability depends on their properties, which have a direct relationship with their size, composition, structure and configuration. Thus, controlling them has turned into the key challenge for researchers of the field.[5,6]

Conventional discontinuous polymerization methods, such as emulsion[6,7], dispersion[8] or spraying[9], do not allow a good control over the final MPs properties. This usually leads to polydispersity and low reproducibility[10,11,12] even at reduced production scales due to the heterogeneous distribution of reactants and temperatures and an insufficient mixing. In the last years, the production of monodisperse particles for biomedical use has stimulated great interest in a myriad of scientific and engineering fields to take advantage of their benefits in controlling drug release rates and obtaining reliable results. Continuous microfluidic devices have introduced different approaches to overcome these previous limitations.[13,14] Micro-sized channels permit to handle fluid flows at the microscale very precisely leading to highly reproducible synthesis and narrow size distributions in the resulting MPs due to an efficient mixing driven by molecular diffusion.[15,16] Microfluidic systems offer also some advantages against classical systems[17]: homogenous reaction conditions, portability, high sensitivity, low energy consumption, highly integrated multifunction and easy scalability.

Droplet microfluidics has been demonstrated to be one of the most efficient microfluidic approaches thanks to the facile control of the reaction conditions and fast MP formation[18]. Two types of flow focusing devices have been considered in the

droplet based microfluidics approach to produce spherical MP[19]: 1) a chip-based flow focusing device with a T or Ψ shaped microchannel integrated on a chip, and 2) a capillary-based flow focusing device (coaxially aligned microcapillaries). Glass-made microchips and capillaries are very expensive, as well as fragile materials.[20,21] Glass manufacturing has the limitations of a complicated welding and gas tight sealing, a difficult integration in a macro-system (connecting to the macro scale) and also any posterior modification is not economically viable. On the other hand, the design and fabrication of microfluidic silicon-based chips could be expensive, labour-intensive and requires clean room facilities. Furthermore, polymerization reactions can easily promote chip blockage, precluding a stable flow. Consequently, while some problems can be overcome by careful choice of the reaction conditions, there is a need for low-cost, modular components that can be easily assembled into flow-focusing devices by users lacking proficiency or access to microfabrication facilities[22]. In this sense, polymeric PTFE coaxially aligned capillaries provide a real alternative thanks to their ease of fabrication and modification, flexibility, re-usability and excellent chemical and mechanical properties and optical transparency.[23,24]

Microparticle precipitation can be provoked by ionic crosslinking[25], temperature induced gelation[26] or by polymerization[27]. Polymerization can be carried out upon heat assisted radical generation or by UV irradiated photopolymerization among other techniques.[28] In this sense, photopolymerization represents a fast process having a precise control over the characteristics of the final polymer after the induction by UV-light lamp exposure[20] avoiding the potential problems that high temperature may provoke on biomolecules used during the synthesis. The use of light emitting diodes (LEDs) holds great promise in the field of photopolymerization due the following advantages[29]: 1) low energy consumption, 2) no ozone release, 3) low heat generation,

4) low operating costs and maintenance, 5) high lifetimes, 6) easy and safe handling, 7) 100% output immediately obtained after turn-on, and 8) easily controlled intensity. Then, the assembly of LED devices and microfluidics to control the polymerization process is an interesting alternative to deal with the controlled production of polymer MPs. Polymerization of droplets can be accomplished upon incorporating a curing agent directly into the droplet, or in the continuous phase. The photoinitiator solubility in the disperse or continuous phase will be the key value to select the polymerization approach. Droplet polymerization can be accomplished during droplet formation, inside the microreactor chip[30,31], or in a totally separated step off-chip[32,33,34]. Time, intensity of light, and reaction components determine the composition, size and properties of the synthetized MPs.[35,36]

MPs prevail as drug delivery vehicles, considering that a large number of products based on polymer MPs have already been commercialized. To name a few: 1) Trelstar® injectable microspheres loaded with triptorelin pamoate and Enantone LP® loaded with Leuprorelin and Lupron® depot loaded with leuprolide acetate for prostate cancer treatment. 2) Sandostatin LAR® depot loaded with octreotide acetate and Somatulin L loaded with lanreotide for acromegaly treatment. 3) Risperdal Consta® depot loaded with risperidone for the treatment of schizophrenia as well as for the longer-term treatment of Bipolar I disorder. 4) Nutropin® depot loaded with recombinant human growth hormone as growth hormone regulator; and 5) Vivitrol® depot loaded with naltrexone for treating alcohol dependence and preventing relapse to opioid dependence. One of the most promising MPs so far for biomedical applications are gel structures.[37] Their capability to respond to several external stimuli such as temperature[38] or pH[39] make them extremely interesting in biomedicine. Among them, microgels based on thermoresponsive polymers are widely studied. One of them, poly(N-

isopropylacrylamide) (PNIPAm) presents a broad variety of opportunities in order to customize the final product according to the desired application[40,41,42]. Crosslinking, monomer and initiator concentration as well as flow rate ratio, irradiation time and intensity of the UV-light source, lead to MPs with completely different properties[43]. Mechanical and thermoresponsive properties of resulted MPs are determined by the fine-tuning of the synthesis variables. Synthesis of hybrid PNIPAm MPs has been conducted in conventional batch type reactors, showing the possibility to combine the function of both thermoresponsive polymers and stimuli sensitive inorganic NPs. For example, Ekici et al.[44] incorporated magnetic iron NPs in hyaluronic acid-PNIPAm nanogels obtaining a double magnetism-temperature responsive system. Moreover, microfluidics allows the precise and controlled encapsulation in MPs of different components from fluorescent dyes[45] to live cells[46,47] that can be useful in drug delivery studies or biosensing[48]. In general, the loading of cargos capable to respond to external stimuli such as light, ultrasound or magnetic fields are very interesting to explore the versatility of hybrid MPs. Superparamagnetic $Fe_3O_4$ NPs (SPIONs) have also been used as triggers for achieving a burst release of lipophilic substances encapsulated in oil cores from core-shell PNIPAm microparticles after induction by alternating magnetic fields[49]. Also, gold nanostructures have been widely used for light-triggered drug release from PNIPAm microcapsules[42]. Wang et al.[50] recently showed the possibility to activate shape transition of Au nanorods-PNIPAm hybrid MPs using high power NIR laser irradiation. Those hybrid MPs were produced in several stages, resulting in a semi-continuous process: 1) Drop formation in continuous flow, 2) Drop sedimentation in stagnant conditions for 5 minutes after collection in order to fine tune the shape and 3) Drop photopolymerization in stagnant conditions under 365 nm UV light during 5 min. Kim et al.[51] also used the same microfluidic approach to generate hollow PNIPAm

microcapsules containing gold nanorods. But in this last case the double-emulsion droplets were incubated in a glass vial for 12 hours at room temperature to complete the polymerization, turning it also as a semi-continuous process, which represents a drawback to increase the productivity. Although a high control over the size and thermoresponsive properties of the MPs were achieved by the reported methods[50,51], the production of PNIPAm hybrid MPs co-loading in the same MP drugs and metal nanoparticles (HGNPs) using a single flow device in continuous fashion by photopolymerization is still lacking. The development of a new flow synthesis approach that enables to address previous drawbacks would accelerate the translation of hybrid MPs applications for their future biomedical use.

Herein, we present a facile, low-cost, and efficient method of producing drug loaded HGNPs-PNIPAm hybrid MPs, capable to tune the structure of the drug carrier MPs in order to achieve different pharmacokinetics in drug delivery applications. A capillary-based flow focusing device with coaxially aligned micro capillaries was coupled to a UV-LED to facilitate the controlled droplet formation and fast polymerization at different synthesis conditions obtaining customized MPs for purpose-specific drug delivery applications. Flow dynamics, reagents ratio and UV exposure time were studied to achieve two types of MPs that behave in a different way, accordingly to the type of drug delivery targeted. The efficient simultaneous loading of a drug and HGNPs is also described. HGNPs were selected as trigger NPs for on-demand light-responsive drug delivery. On its part, bupivacaine was used as a model drug in order to test the pharmacokinetic response of MPs with different shell thicknesses together with the reversible temperature-dependence of hybrid MPs sizes. HGNPs immobilized in the hydrogel network enable the localized heating of the MPs after NIR light illumination, providing the remote control in the permeability of the shell and the triggered release of

bupivacaine. Cytotoxicity analyses were carried out with the materials developed in two different cell lines studying their subcytotoxic concentration and their effect in cell membrane and cell cycle.

## 2 Materials and methods

### 2.1 Materials

N-isopropylacrylamide ≥99% (NIPAM), N,N'-methylenebis(acrylamide) 99% (BIS), Span® 80, hexadecane, ReagentPlus®, 99%, cobalt chloride hexahydrate (ACS reagent grade), sodium citrate tribasic dihydrate (98%), poly(vinylpyrrolidone) (PVP, Mw = 55000 Da), sodium borohydride (99%), gold(III) chloride hydrate (50% Au basis) and bupivacaine hydrochloride monohydrate (99%) were purchased from Sigma-Aldrich. 2,2 Diethoxyacetophenone (DEAP) was purchased from Acros Organics.

### 2.2 Synthesis of hollow gold nanoparticles (HGNPs)

Hollow gold nanoparticles (HGNPs) were synthetized following previous works developed in our group.[52,53] In brief, 400 mL of deionized (DI) water (0.1 % of 0.35 M cobalt chloride hexahydrate) and 1.6 mL of 0.1 M sodium citrate trihydrate were deoxygenated in a two-necked round-bottom flask by bubbling the solution with argon gas for 45 min. Both, 2 mL of 1 wt.% of PVP and 400 μL of 1.0 M sodium borohydride, were added to the previous solution under magnetic stirring forming cobalt NPs. Argon flux and stirring were kept for 15 min. After that, 380 mL of the resulting NPs dispersion was transferred to a beaker containing 120 mL of DI water and 180 μL of 0.1 M gold (III) chloride hydrate under stirring. Magnetic stirring under room temperature conditions was sustained for 30 min until a complete oxidation of the residual cobalt

was produced. A green colored dispersion indicates the presence of HGNPs, which were subsequently washed by several centrifugation steps.

### 2.3 Microreactor characteristics

To produce HGNPs-PNIPAm hybrid microparticles, a coaxial capillary microfluidic device was assembled (Figure 1). The dimensions of the inner and outer capillaries were modified to tune the resulting microparticle sizes. The inner and outer capillaries were made of PEEK (hydrophilic) and PTFE (hydrophobic), respectively. The inner capillary diameter was varied from 150 μm or 25 μm, whereas outer capillary diameter was altered from 560 μm to 790 μm. The dispersed phase (aqueous) was injected at low rates of flow (2.5-30 μL/min) in order to avoid co-laminar flows and unsteady microparticle formation. The inner capillary was coaxially localized under an optical microscope in order get an axisymmetric flow-focusing device where the dispersed phase is surrounded symmetrically by the continuous phase. The coaxial capillary reactor was supported in a polymer housing fabricated by 3D-printing to avoid capillaries misalignment and to favor fluid dynamic reproducibility. In the downstream flow after droplet formation, a UV irradiation provided by a 4.6 W LED (365 nm wavelength) was used to activate the photoinitiator and promote the formation of radicals to polymerize the monomers inside the resulted droplets. LED intensity was modulated in order to obtain the optimum polymerization rate.

Two different syringe pumps (Harvard Apparatus PHD ULTRA™) at selected flow rates were used to control the drop residence time of the injected reagent streams. Finally, microparticles were collected in a water recipient in order to avoid the blockage of the outer tubing.

## 2.4 Preparation of PNIPAm Microparticles

PNIPAm microparticles (MPs) synthesis was based on the protocol published by Choi et al.[54]. However, in this work we have used a facile-fabricated PTFE coaxial microreactor commercially available without clean-room fabrication needs. This platform is combined with a low-cost and environmental friendly UV-LED source not used in the work described by Choi et al. Moreover, chemical composition and reaction conditions were tuned to achieve different pharmacokinetic patterns for specific drug delivery applications. In brief, two immiscible phases were coaxially injected to create a coaxial flow in dripping mode to form w/o monodisperse droplets at the tip of the inner capillary. The disperse aqueous phase was injected through the inner capillary and was composed of the monomer NIPAM (N-isopropylacrylamide) with concentrations between 150 and 250 mg/mL (aqueous solution), and the crosslinker N,N-methylenebisacrylamide (BIS) with a monomer/crosslinker ratio ranging from 25 to 75. On the other hand, the continuous phase was injected through the outer capillary and was composed by hexadecane, Span 80, as surfactant, at a constant concentration (0.043 mg/mL) and 2, 2-diethoxyacetophenone (DEAP) as photoinitiator, ranging its concentrations between 4–50 µL/mL. Flow ratio between both phases was tuned to generate MPs with different chemical and physical properties.

Hybrid HGNPs-PNIPAm MPs were obtained under the same procedure aforementioned but adding different concentrations of HGNPs in the disperse phase stream. Once the hybrid HGNPs-PNIPAm MPs was successfully produced and characterized, the production of a therapeutic vector with a drug permeability function remotely controlled was attempted. The production of the drug loaded hybrid HGNPs-PNIPAm MPs was addressed by a modification of previous HGNPs-PNIPAm MPs protocol, but adding diverse concentrations of bupivacaine hydrochloride monohydrate together with the

NIPAM monomers, crosslinker and HGNPs in the disperse phase stream of the microfluidic system.

### 2.5 Characterization techniques

The characterization of the resulted HGNPs was carried out by Z-Potential measurements at pH=6 in water using a Zeta Plus, Brookhaven Instruments Corporation, NY, USA. Ultraviolet-visible (UV-Vis) absorption spectra were retrieved via a Varian Cary® 50 UV-Visible spectrometer (Agilent Technologies, USA). In addition, Transmission Electron Microscopy (TEM) analyses were developed in a T20-FEI Tecnai thermoionic microscope operated at an acceleration voltage of 200 kV. TEM samples were prepared by dropping 20 µl of sample in Holey carbon coated nickel grid (200 mesh), dried at room temperature.

Characterization of the chemical structure of resulted MPs was carried out by Fourier Transformed Infrared Spectroscopy (FTIR) with a Vertex 70, Bruker with an ATR Golden Gate accessory and by Proton Nuclear Magnetic Resonance ($^1$H-NMR) spectroscopy carried out on a Bruker AV-400 spectrometer operating at 400 MHz using $CDCl_3$ as solvent. In order to demonstrate the proper behavior and reversibility of conformational changes due to temperature variations, the swelling ratio, images and videos were obtained in a multidimensional real time microscope Leica AF6000 LX. The inner presence and distribution of HGNPs inside the polymeric MPs was confirmed by electronic imaging with a Cryogenic Dual Beam Nova 200 (Electron Voltage 200V-30kV; Ion voltage 2kV-30kV). Encapsulation efficiency of gold derived from HGNPs was determined by MP-AES (4100 MP-AES, Agilent Technologies, USA). Calibrations were carried out using Au standards from 0 to 10 ppm in 10 % Aqua regia.

Scanning Electron Microscopy (SEM) images were taken for morphology characterization. Gel Permeation Chromatography (GPC) studies were carried out in

order to study the molecular weight of the resulted samples using a Waters Alliance 2695 HPLC with an evaporative light scattering detector (Waters 2420) and PLgel 5 µm MIXED-C Agilent columns (7.5 mm x 300 mm), using THF (HPLC grade) as eluent (flow 1 mL/min). Calibration was made with poly(methyl methacrylate) standards. Samples were analyzed at 1 mg/mL after filtration using a 0.2 µm PTFE filter.

### 2.6 Bupivacaine release studies

Drug release experiments were carried out in 1 mL of distilled water with 1 mg/mL of loaded hybrid MPs. The samples were kept at 37ºC under stirring and at predefined times they were collected, centrifuged and the content of bupivacaine measured using Gas Chromatography (GC-MS QP2010 SE, Shimadzu). Limonene was used as internal standard.

### 2.7 *In vitro* cell culture studies

The cytocompatibility of solid and hollow MPs loaded with HGNPs and bupivacaine was tested in two different cell types, human dermal fibroblasts and macrophages, through the evaluation of their effects in cell metabolism, apoptosis and cell cycle. Regarding the micrometric size of the synthesized materials, which implies the unfeasibility to be phagocytized by cells, *in vitro* cell cultures were treated with the exudates released from the MPs for 24h in cell culture medium.

Human dermal fibroblasts (Lonza) were grown in Dulbecco's Modified Eagle's Medium (DMEM) high glucose with stable glutamine (Biowest) supplemented with 10% v/v fetal bovine serum (FBS; Thermo Fisher Scientific) and 1% v/v antibiotic-antimycotic (60 µg/mL penicillin, 100 µg/mL streptomycin, and 0.25 µg/mL amphotericin B; Biowest). THP1 human monocytes (ATCC TIB-202; LGC Standards) were cultured in RPMI 1640 with stable glutamine (Biowest) containing 10% v/v FBS

(Thermo Fisher Scientific), 0.1% v/v 2-mercaptoethanol 50 mM (Gibco), 1% v/v non-essential amino acids, 1% v/v HEPES, 1% v/v sodium pyruvate 100 mM and 1% v/v antibiotic-antimycotic, all purchased from Biowest. Phorbol 12-myristate 13-acetate (PMA, Sigma-Aldrich; 1 μM) was added to the culture for 72h to induce the *in vitro* differentiation of monocytes to macrophages. All cell lines were maintained in a humidified atmosphere containing 5% $CO_2$ at 37 °C.

Blue Cell Viability assay (Abnova) was performed to evaluate the effects of MPs exudates (0.01-0.5 mg/mL) on cell metabolism for 24h. After incubation, the reagent (10% v/v) was added to the samples and incubated for 4h at 37 ºC and 5% $CO_2$. Finally, cell viability was evaluated by fluorescence intensity reading (535/590 nm ex/em) in a Synergy HT Microplate Reader (Biotek) through the interpolation of the emission data obtained from the treated and the control (100% viability) samples. The effects of MPs exudates in apoptosis and cell cycle distribution, at the subcytotoxic concentration (0.5 mg/mL) found in the viability assay described above, were evaluated by flow cytometry (Cell Separation and Cytometry Unit, CIBA, IIS Aragon). The analysis of cell apoptosis was developed through a double-staining with Annexin V-FITC and propidium iodide. In brief, after cell incubation with the exudates obtained from solid and hollow MPs loaded with HGNPs and bupivacaine (24h, 37 ºC and 5% $CO_2$), cells were harvested and stained with annexin V-FITC, propidium iodide and annexin V binding buffer. Then, cell suspensions were incubated for 15 min with binding buffer prior to their analysis by flow cytometry (FACSARIA BD equipment and FACSDIVA BD software). The distribution of cell cycle phases after incubation with MPs exudates was carried out by using the PI/RNASE Solution (Immunostep). Briefly, after treatment, cells were harvested, fixed in 70% ice-cold ethanol and kept at 4 ºC at least for 30 min. Then, samples were washed in 2% BSA-PBS, centrifuged (300g, 5 min) and the pellet was

resuspended in the PI/RNASE Solution. After incubation at room temperature for 15 min, flow cytometry (FACSARRAY BD equipment and MODIFIT 3.0 Verity software) was carried out. In both flow cytometry assays, control samples were also run to evaluate cell basal status and compare it with the treated cells.

# 3 Results and discussion

## 3.1 Production of PNIPAm MPs in a capillary-based flow focusing device

The study of single step photopolymerization of PNIPAm MPs was carried out using the capillary-based flow focusing device depicted in Figure 1. As it was described in the materials and methods section, the capillary-based flow focusing device was coupled with a UV LED lamp in order to continuously produce thermoresponsive MPs. Both systems were assembled in a 3-D printed housing to assure a good alignment of the capillaries and an axisymmetric flow-focusing production of MPs. The UV-LED lamp was also assembled in the same housing to preserve the same light distance and thus the same light depth in the capillary in all case studies (Figure 1-b). Previous considerations, capillaries alignment and UV-light distance will be key factors to ensure an excellent MPs production reproducibility. In addition, this production strategy exerts the advantage that each MP is loaded with a similar cargo and that either the polymerization rate or the grade of crosslinking can be easily controlled.

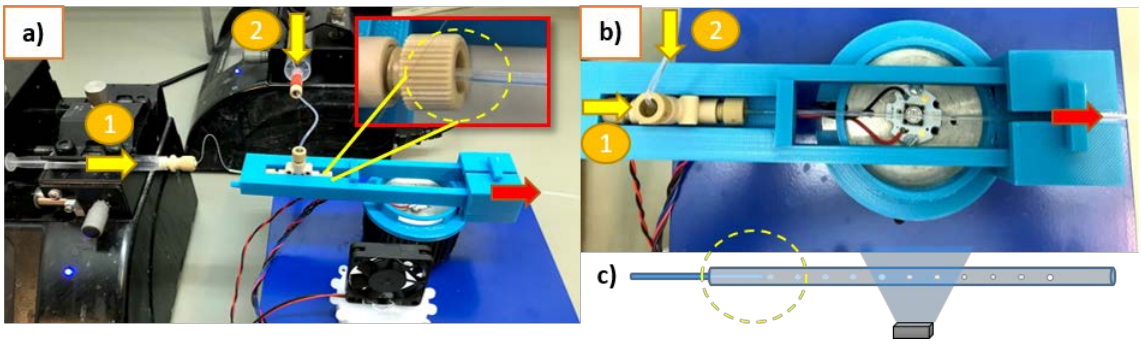

**Figure 1:** Microfluidic device. a) Complete platform used to synthesize all MPs. Upper right corner shows a detail image of the coaxial capillary microfluidic system; b) UV-LED photopolymerization stage coupled to the microfluidic device; c) Scheme of coaxial droplet formation and MPs formation after LED irradiation. (Yellow arrows represents the inlet precursor flows and red arrows guide the already formed MPs outlet flow.

As shown in Figure 1, the capillary-based flow focusing device depended on the use of two immiscible streams. The hydrophilic stream (arrow 1) is injected in the inner capillary (disperse phase) and contains the monomer, crosslinker and the cargo to load inside the thermoresponsive MPs both hollow gold nanoparticles (HGNPs) and bupivacaine. On the other hand, the hydrophobic stream (arrow 2) is the continuous phase injected in the outer capillary. The disperse phase is driven into a UV light transparent capillary and encounters the immiscible carrier stream, which is driven independently. The geometry of the junction where both immiscible phases meet, together with the phases flow rate and physical properties of fluids will determine the local flow field and the interface deformation that promotes droplet breakup in co-flowing streams. The continuous phase stream consists of hexadecane as organic solvent, Span 80® as surfactant, and DEAP as photoinitiator of the polymerization process. In co-flowing streams, the dripping regime occurs at low flow rates of inner and outer fluids and is characterized by the periodic formation of individual droplets that pinch off from the inner capillary tip (Figure 1-c). Once the injected aqueous droplets co-flow with the continuous phase containing the photoinitiator and are introduced in the UV-irradiated region, the photoinitiator is activated and radicals enable the droplet gelification and further polymerization.

Considering previous limitations[50,51] that unable PNIPAm MPs polymerization in continuous flow, we selected dripping regime conditions instead of jetting conditions to

promote a fast polymerization during the drop flow in the microfluidic system. The residence time of formed droplets is usually larger in dripping mode because low flow rates (inner and outer phases) are required. In addition, droplets produced under dripping mode are pinched off near the inner capillary tip, whereas in jetting regime, droplets are pinched off from an extended thread generated downstream of the inner capillary tip. Droplet formation in co-flowing microfluidic systems is sensitive to the viscous shear stress of the external flow and the capillary pressure resisting the deformation of the internal phase.[20] The dimensionless capillary number (Ca) compares the relative importance between the friction force and the surface tension. Then, we considered previous studies of droplet formation in dripping mode using similar fluids[54], to select the fluid dynamic conditions to get stable droplet formation. Several factors such as stream composition or capillary dimensions were tuned in order to control the morphology and the polymerization efficiency of the system. The effect of those parameters will be discussed in the following sections.

### 3.2 Microparticles Morphology and dimensions

It is well accepted that the size of droplet formation in a co-flowing microfluidic device depends on the capillaries dimensions, and inner and outer flow rates. These parameters are highly important because they can modulate the competition between viscous shear stress of the external stream and capillary pressure resisting deformation of the internal stream. In this work, we have selected two different inner and outer capillaries to tune the size of MPs under a stable droplet formation in dripping regime.

Figure 2 shows the averaged MPs diameter obtained under different capillary dimensions and flow rates. In general the most important effect is observed when the external PTFE capillary was modified.

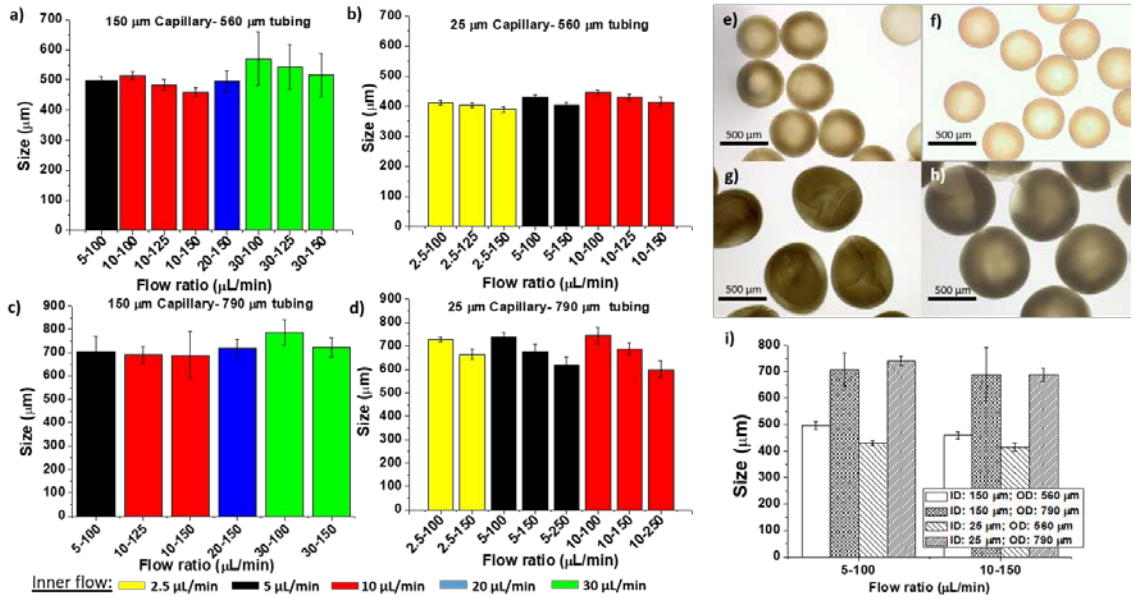


**Figure 2:** Average MPs size depending on flow ratio and inner diameter of the microreator channels. a) and b) show the results for the smallest external PTFE tubing (560 µm) and large (150 µm) and small (25 µm) internal capillary, respectively. c) and d) present the results for the larger PTFE tubing (790 µm) and large (150 µm) and small (25 µm) internal capillary, respectively. Same colors represent the same inner flow. For each of them, from left to right continuous flow increases. Inverted microscope images of MPs synthesized with flow ratio of 5-100 L/min are shown in: e) ID: 150 µm and OD 560 µm; f) ID: 25 µm and OD 560 µm; g) ID: 150 µm and OD 790 µm; h) ID: 25 µm and OD 790 µm. i) Summary and comparison of MPs diameter synthesized with two different flow ratios and all combinations of internal and external tubing diameters.

Smaller outer capillary yielded to microparticles between 400 and 500 µm (Figure 2 b) and a)); while a larger outer capillary diameter generated MPs over 700 µm in diameter (Figure 2 c) and d)). These results can be rationalized by the droplet formation mechanism. The junction close to the inner capillary tip is obstructed by the inner fluid protrusion. The continuous flow close to the protrusion is restricted as the protrusion is enlarged, establishing a pressure gradient across the protrusion. The droplet is pinched off once the pressure gradient in the continuous flow is sufficiently high to overcome

the capillary pressure inside the dispersed drop. Viscous shear forces are usually sufficiently large to pinch off the droplet before it grows to block the outer capillary[55]. Then, the droplet diameter is usually smaller than the outer channel diameter. In addition, the droplet diameter is inversely proportional to the average velocity of the carrier flow because the drag force increases as the continuous phase velocity does[56]. This fact confirms that the MPs diameter increases as the flow rate of the outer stream is decreased when the inner flow rate is kept constant (the drug force is reduced). On the other hand, the inner capillary size mainly affects MPs polydispersity. A more confined droplet formation benefited from a smaller capillary, generating narrower diameter deviation. This is reflected in the different coefficient of variance (CV) of MPs sizes obtained with the four systems studied. While MPs CVs obtained with larger inner capillary (790 μm) have values between 15 nm (when inner flow rate is 10 μL/min) to 100 nm (when continuous phase gets to 30 μL/min), a maximum variance of 30 nm is achieved in experiments when using 25 μm inner capillary. Similar results were previously observed with analogous platforms.[57] Dripping frequency production (*f*) for all samples ranges between 7.5 Hz to 0.2 Hz depending on the inner flow rate and final size of MPs. Slow flow rate (2.5 μL/min) and large final MPs (~700 μm) lead to slow droplet formation and frequencies around 0.2 Hz. However, increasing the inner flow rate up to 30 μL/min and confining the size of the outer capillary, and thus the final MPs size (~400 μm), provoked a faster droplet formation and frequencies over 7.5 Hz. It is of paramount importance to highlight that this low dripping frequency was required in order to get a complete polymerization reaction in continuous fashion, a fact that is novel in this work.

According to the aforementioned polymerization requirements, it is essential to achieve certain level of polymerization rate in order to obtain stable MPs with a competent

functionality for a potential biomedical use. This fact, together with the fluid dynamic restrictions required to achieve a stable droplet generation limit the available phase flow rates. In this work a single LED source has been considered, however using several LEDs in series would potentially increase the irradiation time allowing the use of larger flow rates.

It has been demonstrated that droplet size in coaxial flow platforms with flow ratios within our working limits do not change significantly[21]. However, it can still have small effects on the final MPs sizes. Statistical analysis of our results (Figure S1) showed some significant differences in almost all flow ratio combinations suggesting that as mentioned before, keeping the same inner flow, the increase in the continuous flow rate for all samples led to a slight decrease in the final MPs size. In all cases, monodisperse MPs were obtained with variations less than 15 % of their size in the worst-case scenario (150 µm inner capillary) but with average CV of 2.5 % in the most stable cases (25 µm inner capillary).

### 3.3 Polymerization efficiency and thermoresponsive properties

Photopolymerization reactions depend on a set of different variables (monomer, photoinitiator and crosslinker concentrations and LED irradiance and time of irradiation) and some of them were studied using this co-flowing microfluidic device. Considering that the main goal of this research was to produce MPs with on-demand light-responsive drug delivery ability and allow a remote control of the polymeric shell permeability, we attempted the analysis of volume ratio shrinkage in the resulted MPs. This parameter was also selected as a key factor to analyze the polymerization efficiency and thermo-responsive properties. It must be highlighted that either an unsuccessful or limited polymerization yield can induce MP collapse, aggregation or a

scarce volume shrinkage upon a temperature variation in the lower critical solution temperature (LCST) range.

On the other hand, crosslinking agent entails a key role in the shrinkage behavior of any hydrogel. Higher concentration of crosslinking molecules among formed polymer chains leads to steric difficulties to achieve a complete shrinkage of the hydrogel from its swollen hydrated state to its shrunken dehydrated form.

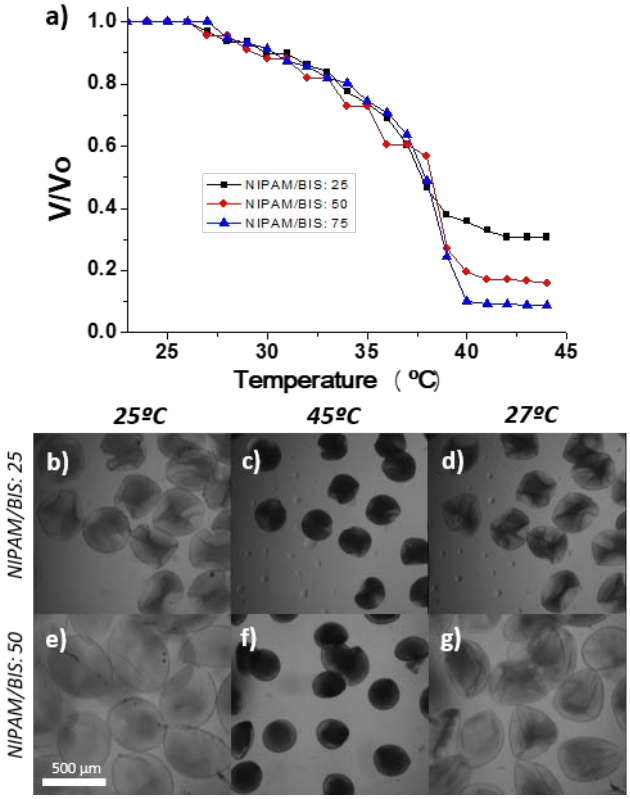


**Figure 3:** Volume change with temperature for a) MPs synthetized with 250 mg/mL monomer concentration and 40 µL DEAP and different crosslinker concentrations; b) to g) Time-lapse microscopy images of MPs synthetized with the same conditions at different temperatures. All samples were synthetized under flow ratio of 5/100 µL/min, inner capillary diameter: 25 µm and outer capillary: 560 µm.

Figure 3 a) represents the volume ratio with temperature obtained for three different samples containing 25, 50 and 75 monomer-crosslinker NIPAM-BIS ratio, respectively.

The results confirm that all MPs produced show a fast response to environmental temperature. It is relevant that dramatic changes occur between 32-39ºC (LCST of PNIPAm is 32ºC). This may be attributed to polydispersity in the polymer chain lengths and crosslinking degree[58,59]. It was also confirmed that the highest the NIPAM-BIS ratio, the largest the rate of volume change of the photo-polymerized MPs is. The volume change in PNIPAm MPs is rationalized because MPs are in a swollen and hydrophilic state below the LCST that is switched to a shrunken and hydrophobic state above the LCST. The state transition was studied in a time-lapse inverted microscope at different temperatures. Figures 3 b) to g) depict representative optical images at different environmental temperatures, where the dramatic reduction of MPs size above the LCST is clearly observed as well as the reversibility of this process once the temperature decreases. Similar behavior was also observed when monomer concentration and monomer/crosslinker ratios (NIPAM/BIS) were modified (Figure S2) confirming the thermoresponsive behavior of the final polymer conforming MPs.

Polymerization efficiency is related to the polymerization rate and it has direct influence in the length of the polymeric chains formed and the possibility to collapse and reduce their volume and size under high temperatures. Figure 4 shows the effect of monomer (NIPAM) and photoinitiator (DEAP) concentration on final molecular weight of resulted MPs and their ability to reduce their volume under temperature variations.

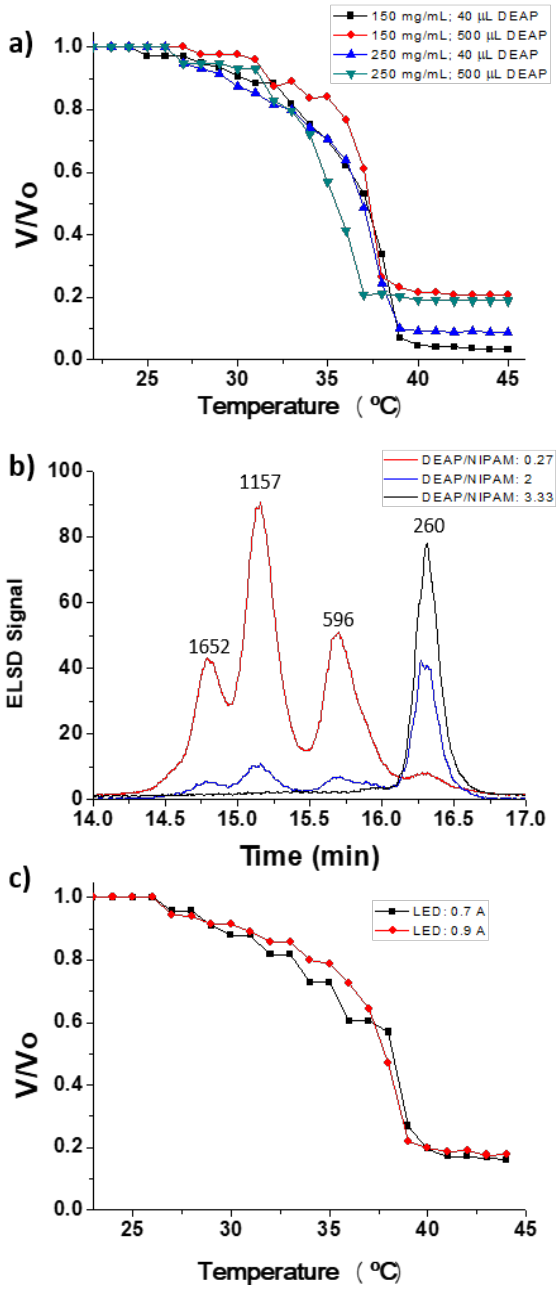


**Figure 4:** a) Volume ratio observed in samples synthesized with different monomer and photoinitiator concentrations; b) GPC results for three different samples with different DEAP/monomer ratio; c) Volume ratio shown for two samples polymerized with two different LED light irradiation intensities.

Figure 4 a) demonstrates that the photoinitiator (DEAP) concentration is crucial to achieve a desired grade of polymerization that is high enough to endow MPs formation with the appropriate rate of volume change and thermosensitive behavior. A high DEAP

concentration leads to a high concentration of radical species that initiate polymerization. However, the fastest the polymerization is, the shorter the polymer chains formed and then, the less the volume change when the environmental temperature increases. This observation was also confirmed by Gel Permeation Chromatography (GPC) (Figure 4 b). The GPC chromatogram provides the molecular weight distribution of the resulting species, labeling the main molecular weight peaks (Figure 4-b). According to GPC analysis, the molecular weight of the resulted polymer is lower as the photoinitiator concentration is increased because a high density of monomer building blocks is activated by the radical species. This fact was also evidenced by inverted microscopy, where optical images taken at different environmental temperatures depicted a significant shrinkage as the photoinitiator content was decreased (Figure S3). On the other hand, the activity of the photoinitiator molecules is determined by their stimulation source, the UV-LED light in our system. The irradiance of LED source determines the velocity of the polymerization process leading to different polymer chain lengths and thus to different photothermal properties. There is an intensity threshold that determines the minimum intensity necessary in order to obtain rigid and mechanically stable MPs below the one where no enough polymer chains were formed, and MPs did not keep their shape after exiting the microfluidic platform. Intensities from 0.2 to 0.9 A were used in our study finding the threshold described before set at 0.7 A. At intensities of 0.2 and 0.4 A no MPs formation took place and easily breakable MPs were obtained, respectively. However, above 0.7 A no significant changes were observed when UV-LED light intensity was increased to 0.9 A (Figure 4 c) in our system.

As the polymerization is initiated at the interface of the aqueous/organic phase of detached droplets, the diffusion of radical species that conduct the polymerization

reaction might have a relevant role in the MPs structure. In these terms, hollow or solid MPs could be produced depending on the radical species droplet internalization. Kim et al.[31] corroborated the relationship of a high polymerization ratio with the improved mechanical strength of the resulted MPs. Long irradiation times, high DEAP concentration and high irradiation intensity favored to obtain a solid structure and mechanically resistant MPs. However, the highly solid MPs obtained under these conditions resulted in low shrinkage ratios (~24 v/v%).

The polyethylene glycol diacrylate (PEGDA) photopolymerization reaction from a droplet microfluidic device emulsification process was also studied by Filatov et al.[36] showing the importance of the photoinitiator concentration and the reaction time in the final core-shell structure and MPs resistance. However, a plateau of time reaction exists at very high photoinitiator concentration where increasing photoinitiator concentration does not lead to faster polymerization reaction. On the other hand, when the monomer concentration increases, more monomer molecules are available at the droplet surface leading to thicker MP shells and thus more mechanically resistant MPs. This is explained due to a faster polymerization process with the same reaction time.

Considering our previous remarks, it was devised the formation of two types of MPs with a different internal structure and good mechanical properties, where the density of polymeric chains was tuned in order to modulate the void fraction and the rate of volume shrinkage. Figure 5 shows some of the most representative MPs produced by tuning the polymerization rate, either by modifying the flow rate of the continuous outer phase or the photoinitiator concentration. MPs produced at the opposite conditions were discarded because they unfeasible applicability. That is, MPs produced with the smallest flow rate and photoinitiator concentration (Figure 5-a), because they were not mechanically stable. On the other hand, MPs produced at the highest flow rate and

photoinitiator concentration (Figure 5-d), because of the high density of polymeric chains and rigidity would seriously affect the rate of volume shrinkage. As a result, intermediate conditions were selected as the proper ones in order to load the cargo and study the temperature assisted drug release (Figure 5 b-c).

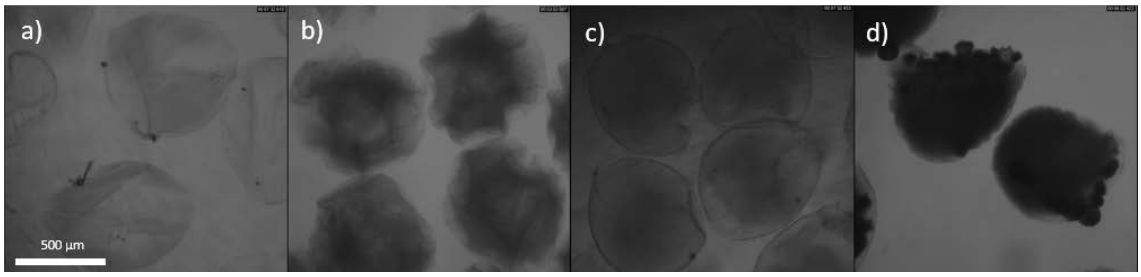


**Figure 5:** From left to right MPs synthesized with monomer concentration of 150 mg/mL (a) and b)) and 250 mg/mL (c) and d)). Images a) and c) were synthetized with 40 µL of photoinitiator (DEAP); while 500 µL of photoinitiator (DEAP) were used in images b) and d).

Transition temperature in drug delivery applications may lead to different drug release profiles which could be appropriate for a broad variety of disease treatments. This tuning of LCST can be achieved by combining different monomers in the polymeric structure. It has been previously demonstrated that the presence of diverse functional groups at the side chains of the polymer chain results in variations of hydrophobicity and thus polymer-water interactions[60]. Acrylamide monomer has been widely used in order to increase the transition temperature in PNIPAm-based polymers. The lack of isopropyl groups in its side chain increases water-polymer interactions making more energy necessary to fold the polymer chains.

In our proposed microfluidic platform, this varied monomer combinations driven to obtain customized thermoresponsive MPs with desired LCST is easy to carry out. We demonstrated that adding Acrylamide (AAm) as co-monomer the LCST of the resulting MPs can be easily modified (See Figure S4). LCSTs for MPs with different acrylamide percentages are summarized in Table 1.

**Table 1:** LCST summary for P(NIPAM-co-AAm) MPs. LCST were selected as the 50% of volume change during temperature increase. Three different samples were analyzed for each condition

| ***Sample*** | **150 mg/mL** | **250 mg/mL** |
|---|---|---|
| *PNIPAm* | 37.3 ± 0.8°C | 35.5 ± 0.5 °C |
| *P(NIPAM-co-AAm) 7 %* | 38.7 ± 0.7 °C | 39.1 ± 0.7 °C |
| *P(NIPAM-co-AAm) 10 %* | 39.1 ± 0.4°C | 39.5± 0.6 °C |

In all cases, the addition of extra AAm monomers leads to higher LCST over body temperature making them ideal for triggered on-demand drug delivery applications. Therefore, the proposed microfluidic platform allows easily modifying the resulting MP particle size including its LCST and composition depending on the needs.

### 3.4 HGNPs encapsulation and NIR triggered drug delivery

It is well known that hollow gold nanoparticles (HGNPs) present excellent plasmonic properties based on their Surface Plasmon Resonance (SPR) band with a maximum at ~808 nm. This property has been widely used in biomedical applications because of the coincidence with the water window absorption. Water molecules and tissues have reduced light absorption at wavelengths around 808 nm making HGNPs the perfect candidates for NIR light excitation in light-activated biomedical treatments. Thus, we took advantage of the optical properties of HGNPs in order to obtain hybrid thermoresponsive MPs for triggered drug delivery.

For this, we added the separately prepared HGNPs in the disperse phase of the coaxial flow microfluidic device to translate the synthesis conditions optimized in the previous section. Based on previous works where nanoparticles with photothermal properties[61,50] were encapsulated, the concentration of HGNPs was set at 10 mg/mL. Further, we confirmed their NIR responsive effect under laser irradiation (2.2 W/cm$^2$; λ= 808 nm). (Figure 6)

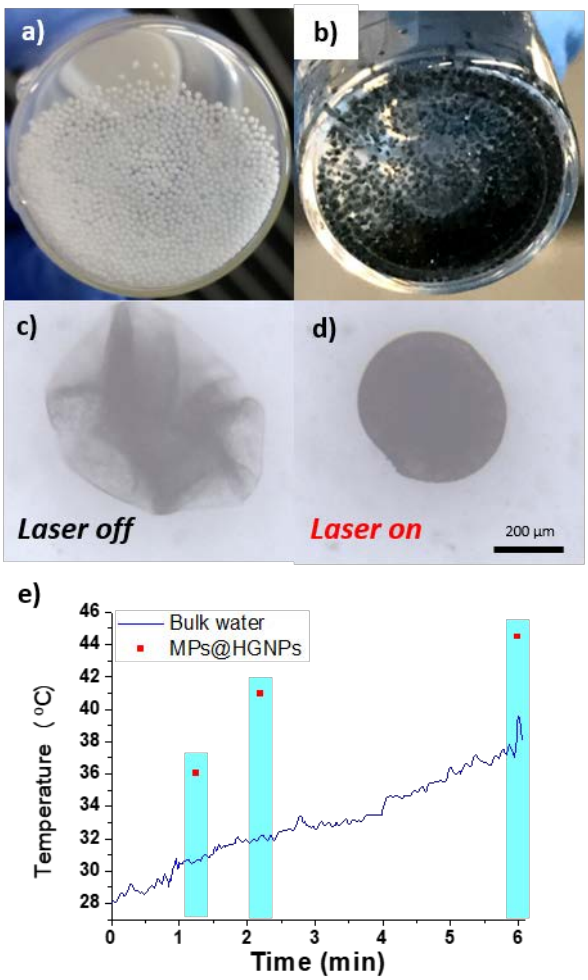


**Figure 6:** a) and b) PNIPAm MPs without and with HGNPs; c) and d) Optical microscopy images without and with laser irradiation (2.2 W/cm$^2$); e) Time heating evolution of bulk water in presence of MPs@HGNPs. Red dots represent selected times where MPs@HGNPs cluster (i.e., agglomerated MPs) temperature was measured.

Figure 6 a) and b) show the notable color differences when HGNPs were loaded in PNIPAm MPs (66% HGNPs encapsulation efficiency obtained by MP-AES analysis). It must be highlighted than the proposed production approach enables a selective loading of HGNPs, where the dose of HGNPs can be easily modified by tuning their concentration in the disperse phase stream. No size and shape modifications were observed after adding HGNPs to the disperse phase together with the monomer molecules. The continuous phase wraps the droplet and inhibits the diffusion of HGNPs

during the polymerization process. It was selected an IR laser with a wavelength of 808 nm (2.2 W/cm$^2$) to heat the MPs@HGNPs owing to its larger penetration depth compared to the one reached with visible light. MPs@HGNPs were illuminated at 25ºC with the laser to study the rate of volume shrinkage. As it is depicted in Figure 6d, upon laser illumination, MPs@HGNPs shrunk due to a local temperature increase caused by the light to heat transduction generated by the HGNPs. This result confirms the new functionality of the proposed hybrid MPs, where the MP collapse can be triggered by externally applied NIR illumination. It is also interesting to remark that the optical properties of HGNPs were not modified during the loading and polymerization process under the presence of highly oxidant radical species. The shape transition during the MPs@HGNPs collapse upon laser heating and the reversibility of the process once the laser was switched off were also recorded in a single MP using time-lapse microscopy, obtaining that the collapse occurs instantaneously at the selected laser intensity (See Supporting Movie S1).

Temperature rise under NIR laser irradiation is plotted in Figure 6 e). Due to the size of MPs studied, MPs@HGNPs settle in the bottom of the vial and temperature of bulk water around them and the one of the MPs@HGNPs themselves were separately tested. It was observed that the bulk water temperature raised slowly under the presence of MPs@HGNPs, however, it was the MPs@HGNPs cluster itself the one which suffered an abrupt temperature rise. Temperature was monitored with a thermocouple located in the middle of MPs@HGNPs cluster at selected times. It increased clearly above the aqueous medium temperature almost 10 ºC reaching 45 ºC after 6 minutes of irradiation. This suggested a local heating effect in the surroundings of HNPs loaded MPs, what together with the shrunk morphology observed under optical microscopy confirm their suitability for triggered on demand drug delivery applications.

As it was described in the previous section, two different polymeric MPs were selected for drug loading and release studies obtained under distinct synthesis conditions. The porosity of drug delivery vectors determine not only their drug loading capacity but also drug release profile once they are in the application environment. In our case, two kinds of MPs determined as hollow (*NIPAM: 250 mg/mL and DEAP: 40 µL*) and solid (*NIPAM: 150 mg/mL and DEAP: 500 µL*) were studied. Even with the same size, the structure of the MPs studied was different: hollow MPs were more fragile and with a thinner polymeric shell while solid MPs had a polymeric dense structure even in their core reducing their porosity but increasing their mechanical strength. Bupivacaine was selected as model drug due to its common applications in peripheral nerve blocking in pain treatment and due to its inert behavior under UV-LED light irradiation (See Figure S6).

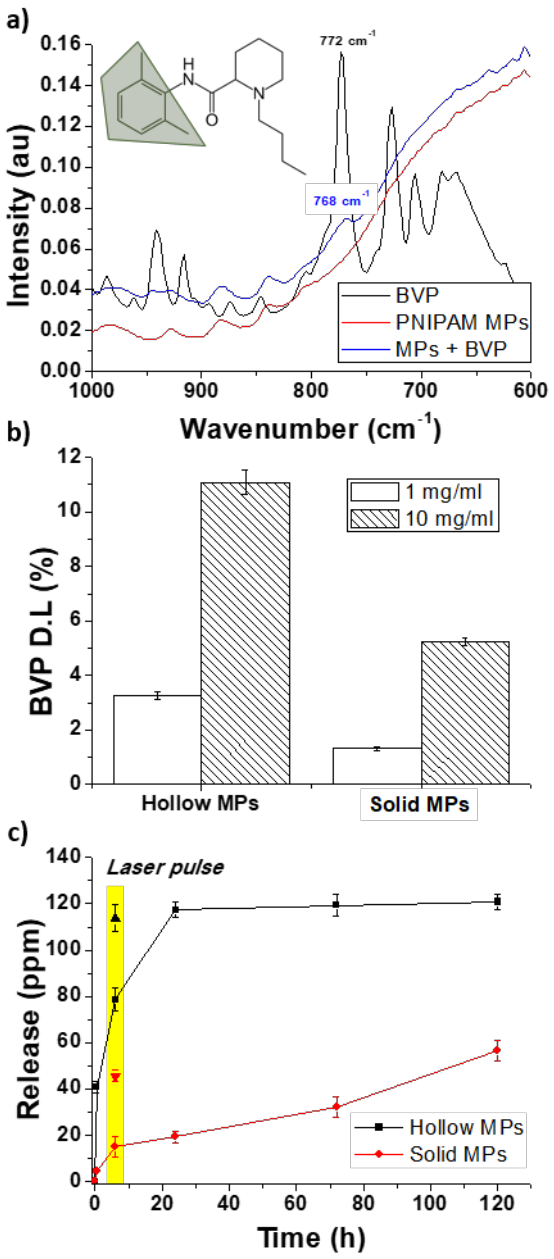


**Figure 7:** a) FTIR spectra of Bupivacaine (BVP), PNIPAm-based MPs and BVP loaded MPs; b) Drug loading of hollow and solid MPs after adding two different BVP concentrations in the disperse phase; c) Cumulative release profile for both solid and hollow MPs. Yellow band shows the burst release under a single laser pulse irradiation. Upward black triangle and downward red triangle represent the bupivacaine release value for Hollow and Solid microparticles, respectively.

Figure 7 a) shows the FTIR spectra for empty and BVP loaded MPs together with free BVP. Here, we can observe the existence of a shift in the peak (772 to 768 $nm^{-1}$) associated to the aromatic ring of BVP molecule suggesting an interaction between the polymer and the bupivacaine molecules present in the sample. In Figure 7 b) drug loadings of BVP for hollow and solid MPs are compared. The higher the BVP content is, the higher the final BVP content in the sample. However, notable differences are present comparing hollow and solid MPs. While solid MPs are composed by an inner entangled core of polymer chains, hollow MPs have more empty space available to adsorb the drug inside, what is clearly shown in our case. Also, the thickness of the MPs wall has an important effect in the release profile as depicted in Figure 7 c). The drug release at body temperature for hollow MPs is faster than the one obtained for solid ones. Bupivacaine molecules interact strongly with polymer chains inside solid MPs probably due to hydrogen bonding and hydrophobic Van der Waals interactions leading to a sustained drug release. These two drug delivery vectors can be used for different purposes. Khan et al.[57] had already observed a similar behavior in the simultaneous release of two drugs (i.e., ketoprofen and ranitidine HCl) from MPs with different polymer density. A faster release was achieved when crosslinker and monomer concentrations decreased.

### 3.5 Cell viability, apoptosis and cycle evaluation

Due to the MPs sub-millimetric size and inability to be internalized by cells and their proposed applications as depots in local subcutaneous or intramuscular triggered drug delivery, the cytocompatibility studies were carried out in two different cell lines (phagocytic macrophages and human dermal fibroblasts) analyzing the exudates released by the MPs during 24h as described in the materials and methods section. Figure 8 presents cell viability results for concentrations from 0.1 to 0.5 mg/mL and the

corresponding bupivacaine concentration. High cell viability (> 70%) was observed for all MPs concentration tested for both solid and hollow MPs exudates showing more compatibility than free BVP in human fibroblast. Following studies were developed at a MPs concentration of 0.5 mg/mL as it was considered as subcytotoxic dose following the ISO 10993-5 standard, which states a viability of 70% as the threshold for considering non-cytotoxic concentrations.[62]

Cell apoptosis studies by flow cytometry were selected to show the potential cell membrane effect caused by the MPs exudes (Table 2). The incubation of the two cell lines (TPH1 macrophages and human dermal fibroblasts) at the subcytotoxic concentration (0.5 mg/mL) with MPs exudates loaded with HGNPs and BVP did not show remarkable changes compared to non-treated samples. Only macrophages showed a slight increase in necrosis and late apoptosis for hollow and solid loaded MPs, respectively (<3%) and a consequent decrease in cellular viability (<4%).

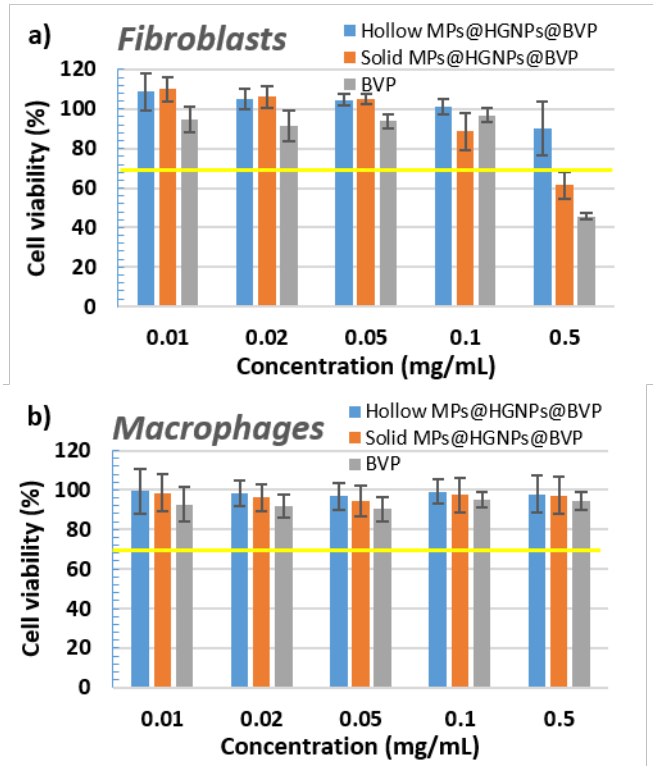


**Figure 8:** Cytotoxicity results for two cell lines: a) Human fibroblasts and b) macrophages for two different shell thickness MPs denominated solid and hollow MPs loaded with HGNPs and Bupivacaine; and free bupivacaine. Mean values and SD obtained from fives samples.

**Table 2:** Apoptosis results obtained by flow cytometry

| | Control | Exude solid MPs | Exude hollow MPs |
|---|---|---|---|
| | Macrophages (%) | | |
| Necrosis | 4.43 | 2.09 | 7.41 |
| Late apoptosis | 1.72 | 5.74 | 2.58 |
| Early apoptosis | 0.59 | 1.44 | 1.14 |
| Viability | 93.26 | 90.74 | 88.87 |
| | Fibroblasts (%) | | |
| Necrosis | 0.51 | 0.33 | 0.38 |
| Late apoptosis | 1.99 | 2.47 | 2.01 |
| Early apoptosis | 3.05 | 3.18 | 2.76 |
| Viability | 94.44 | 94.02 | 94.85 |

Cell cycle studies are depicted in Table 3. Cell treatment for 24 h with HGNPs-BVP loaded PNIPAm MPs exudates at subcytotoxic doses (0.5 mg/mL) did not display accentuated effects on cell cycle. A slight increase in G2 phase in macrophages (<2%)

and in S phase in fibroblasts (<4%) are the only changes observed after treatment compared to control samples. Therefore, at the doses tested the exudates released by the MPs here prepared did not show cytotoxicity, cell-cycle arrest or apoptotic induction.

**Table 3:** Cell cycle results obtained by flow cytometry

| | Control | Exude solid MPs | Exudate hollow MPs |
|---|---|---|---|
| | Macrophages (%) | | |
| G1 | 55.72 | 53.44 | 54.11 |
| S | 13.32 | 13.49 | 13.41 |
| G2 | 30.96 | 33.08 | 32.48 |
| | Fibroblasts (%) | | |
| G1 | 45.72 | 43.83 | 44.19 |
| S | 31.34 | 35.99 | 35.17 |
| G2 | 22.94 | 20.18 | 20.64 |

## 4 Conclusions

Summing up, in this work we obtained thermosensitive light-responsive hybrid MPs loaded with an anesthetic drug using an innovative one-step continuous synthesis method. A simple, versatile and highly productive microfluidic synthesis was developed for this purpose. The influence of the reaction conditions in the final MPs characteristics was analyzed. The presence of plasmonic HGNPs in the MPs was demonstrated as potential trigger for drug delivery applications in biomedicine. In order to test drug loading and release behavior, bupivacaine was selected as a drug of interest and the interaction, loading capacity and release studies confirmed the suitability of the MPs obtained for reaching tunable drug delivery profiles. Finally, cytotoxicity assays showed a subcytotoxic dose of 0.5 mg/mL further used to study the cell metabolism and cell cycle showing no remarkable influence in any of the cell lines studied. Altogether, make this microfluidic device suitable for MPs synthesis for further local treatment applications such as the treatment of chronic pain where an anesthetic depot could be

externally activated to release its cargo on demand. Further improvements such as different capillary sizes, LED irradiation arrangements or introduction of other drug molecules or inorganic nanoparticles would be the next steps to expand the possibilities of this novel microfluidic device.

## 5 Acknowledgments

Financial support from the ERC Consolidator Grant program (ERC-2013-CoG-614715, NANOHEDONISM) is gratefully acknowledged. CIBER-BBN is an initiative funded by the VI National R&D&i Plan 2008-2011 financed by the Instituto de Salud Carlos III with the assistance of the European Regional Development Fund.

## 6 Associated content

Supporting figures are available in Supporting Information File.

Additional information of the reversible MPs swelling under laser irradiation is presented in Supporting Movie_S1.

## 7 References

(1) Choi, A.; Seo, K. D.; Kim, D. W.; Kim, B. C.; Kim, D. S. Recent Advances in Engineering Microparticles and Their Nascent Utilization in Biomedical Delivery and Diagnostic Applications. *Lab Chip* **2017**, *17* (4), 591–613.

(2) Jung, S.; Choi, C. H.; Lee, C. S.; Yi, H. Integrated Fabrication-Conjugation Methods for Polymeric and Hybrid Microparticles for Programmable Drug Delivery and Biosensing Applications. *Biotechnol. J.* **2016**, *11* (12), 1561–1571.

(3) Xu, Q.; Hashimoto, M.; Dang, T. T.; Hoare, T.; Kohane, D. S.; Whitesides, G. M.; Langer, R.; Anderson, D. G. Preparation of Monodisperse Biodegradable

Polymer Microparticles Using a Microfluidic Flow-Focusing Device for Controlled Drug Delivery. *Natl. Inst. Heal. Public Access* **2010**, *5* (13), 1575–1581.

(4) Jiang, W.; Li, M.; Chen, Z.; Leong, K. W. Cell-Laden Microfluidic Microgels for Tissue Regeneration. *Lab Chip* **2016**, *16* (23), 4482–4506.

(5) Berkland, C.; King, M.; Cox, A.; Kim, K.; Pack, D. W. Precise Control of PLG Microsphere Size Provides Enhanced Control of Drug Release Rate. *J. Control. Release* **2002**, *82* (1), 137–147.

(6) Agrawal, G.; Agrawal, R. Stimuli-Responsive Microgels and Microgel-Based Systems: Advances in the Exploitation of Microgel Colloidal Properties and Their Interfacial Activity. *Polymers (Basel).* **2018**, *10* (4).

(7) Chan, K. M. C.; Li, R. H.; Chapman, J. W.; Trac, E. M.; Kobler, J. B.; Zeitels, S. M.; Langer, R.; Karajanagi, S. S. Functionalizable Hydrogel Microparticles of Tunable Size and Stiffness for Soft-Tissue Filler Applications. *Acta Biomater.* **2014**, *10* (6), 2563–2573.

(8) Cirillo, G.; Iemma, F.; Spizzirri, U. G.; Puoci, F.; Curcio, M.; Parisi, O. I.; Picci, N. Synthesis of Stimuli-Responsive Microgels for in Vitro Release of Diclofenac Diethyl Ammonium. *J. Biomater. Sci. Polym. Ed.* **2011**, *22* (4–6), 823–844.

(9) Bazzano, M.; Latorre, D.; Pisano, R.; Sangermano, M.; Woerner, M. Nano-Structured Polymeric Microparticles Produced via Cationic Aerosol Photopolymerization. *J. Photochem. Photobiol. A Chem.* **2017**, *346*, 364–371.

(10) Vladisavljević, G. T.; Williams, R. A. Recent Developments in Manufacturing Emulsions and Particulate Products Using Membranes. *Adv. Colloid Interface Sci.* **2005**, *113* (1), 1–20.

(11) Charcosset;, C.; Fessi, H. MEMBRANE EMULSIFICATION AND

MICROCHANNEL EMULSIFICATION PROCESSES. *Rev. Chem. Eng.* **2005**, *21*, 1–32.

(12) De Geest, B. G.; Urbanski, J. P.; Thorsen, T.; Demeester, J.; De Smedt, S. C. Synthesis of Monodisperse Biodegradable Microgels in Microfluidic Devices. *Langmuir* **2005**, *21* (23), 10275–10279.

(13) Choi, C. H.; Weitz, D. A.; Lee, C. S. One Step Formation of Controllable Complex Emulsions: From Functional Particles to Simultaneous Encapsulation of Hydrophilic and Hydrophobic Agents into Desired Position. *Adv. Mater.* **2013**, *25* (18), 2536–2541.

(14) Ma, S.; Thiele, J.; Liu, X.; Bai, Y.; Abell, C.; Huck, W. T. S. Fabrication of Microgel Particles with Complex Shape via Selective Polymerization of Aqueous Two-Phase Systems. *Small* **2012**, *8* (15), 2356–2360.

(15) Nosrati, Z.; Li, N.; Michaud, F.; Ranamukhaarachchi, S.; Karagiozov, S.; Soulez, G.; Martel, S.; Saatchi, K.; Häfeli, U. O. Development of a Coflowing Device for the Size-Controlled Preparation of Magnetic-Polymeric Microspheres as Embolization Agents in Magnetic Resonance Navigation Technology. *ACS Biomater. Sci. Eng.* **2018**, *4* (3), 1092–1102.

(16) Xu, J. H.; Zhao, H.; Lan, W. J.; Luo, G. S. A Novel Microfluidic Approach for Monodispersed Chitosan Microspheres with Controllable Structures. *Adv. Healthc. Mater.* **2012**, *1* (1), 106–111.

(17) Sebastian, V.; Arruebo, M. *Microfluidic Production of Inorganic Nanomaterials for Biomedical Applications*; Elsevier Inc., 2018.

(18) Dong, H.; Tang, G.; Ma, T.; Cao, X. One-Step Fabrication of Inorganic/Organic Hybrid Microspheres with Tunable Surface Texture for Controlled Drug Release Application. *J. Mater. Sci. Mater. Med.* **2016**, *27* (1), 7.

(19) Seo, K. D.; Kim, D. S.; Sánchez, S. Fabrication and Applications of Complex-Shaped Microparticles via Microfluidics. *Lab Chip* **2015**, *15* (18), 3622–3626.

(20) Choi, C.-H.; Jung, J.-H.; Kim, D.-W.; Chung, Y.-M.; Lee, C.-S. Novel One-Pot Route to Monodisperse Thermosensitive Hollow Microcapsules in a Microfluidic System. *Lab Chip* **2008**, *8* (9), 1544–1551.

(21) Kanai, T.; Ohtani, K.; Fukuyama, M.; Katakura, T.; Hayakawa, M. Preparation of Monodisperse PNIPAM Gel Particles in a Microfluidic Device Fabricated by Stereolithography. *Polym. J.* **2011**, *43* (12), 987–990.

(22) Xi, W.; Kong, F.; Yeo, J. C.; Yu, L.; Sonam, S.; Dao, M.; Gong, X.; Lim, C. T. Soft Tubular Microfluidics for 2D and 3D Applications. *Proc. Natl. Acad. Sci.* **2017**, *114* (40), 10590–10595.

(23) Ren, K.; Dai, W.; Zhou, J.; Su, J.; Wu, H. Whole-Teflon Microfluidic Chips. *Proc. Natl. Acad. Sci.* **2011**, *108* (20), 8162–8166.

(24) Nge, P. N.; Rogers, C. I.; Woolley, A. T. Advances in Microfluidic Materials, Functions, Integration and Applications. *Chem. Rev.* **2013**, *113* (4), 2550–2583.

(25) Hu, Y.; Wang, S.; Abbaspourrad, A.; Ardekani, A. M. Fabrication of Shape Controllable Janus Alginate/PNIPAAm Microgels via Microfluidics Technique and Off-Chip Ionic Cross-Linking. *Langmuir* **2015**, *31* (6), 1885–1891.

(26) Velasco, D.; Tumarkin, E.; Kumacheva, E. Microfluidic Encapsulation of Cells in Polymer Microgels. *Small* **2012**, *8* (11), 1633–1642.

(27) Seiffert, S.; Weitz, D. A. Controlled Fabrication of Polymer Microgels by Polymer-Analogous Gelation in Droplet Microfluidics. *Soft Matter* **2010**, *6* (14), 3184.

(28) Li, W.; Zhang, L.; Ge, X.; Xu, B.; Zhang, W.; Qu, L.; Choi, C. H.; Xu, J.; Zhang, A.; Lee, H.; Weitz, D. A. Microfluidic Fabrication of Microparticles for

Biomedical Applications. *Chem. Soc. Rev.* **2018**, *47* (15), 5646–5683.

(29) Dietlin, C.; Schweizer, S.; Xiao, P.; Zhang, J.; Morlet-Savary, F.; Graff, B.; Fouassier, J. P.; Lalevée, J. Photopolymerization upon LEDs: New Photoinitiating Systems and Strategies. *Polym. Chem.* **2015**, *6* (21), 3895–3912.

(30) Sivakumaran, D.; Mueller, E.; Hoare, T. Microfluidic Production of Degradable Thermoresponsive Poly(: N -Isopropylacrylamide)-Based Microgels. *Soft Matter* **2017**, *13* (47), 9060–9070.

(31) Kim, Y. S.; Lee, H. M.; Kim, J. H.; Joo, J.; Cheong, I. W. Hydrogel Adsorbents of Poly(N-Isopropylacrylamide-Co-Methacryloyloxymethyl-12-Crown-4) for Li+recovery Prepared by Droplet Microfluidics. *RSC Adv.* **2015**, *5* (14), 10656–10661.

(32) Cheng, C. J.; Chu, L. Y.; Ren, P. W.; Zhang, J.; Hu, L. Preparation of Monodisperse Thermo-Sensitive Poly(N-Isopropylacrylamide) Hollow Microcapsules. *J. Colloid Interface Sci.* **2007**, *313* (2), 383–388.

(33) Ge, X. H.; Huang, J. P.; Xu, J. H.; Luo, G. S. Controlled Stimulation-Burst Targeted Release by Smart Decentered Core-Shell Microcapsules in Gravity and Magnetic Field. *Lab Chip* **2014**, *14* (23), 4451–4454.

(34) Mou, C. L.; Ju, X. J.; Zhang, L.; Xie, R.; Wang, W.; Deng, N. N.; Wei, J.; Chen, Q.; Chu, L. Y. Monodisperse and Fast-Responsive Poly(N -Isopropylacrylamide) Microgels with Open-Celled Porous Structure. *Langmuir* **2014**, *30* (5), 1455–1464.

(35) Park, S.; Kim, D.; Ko, S. Y.; Park, J. O.; Akella, S.; Xu, B.; Zhang, Y.; Fraden, S. Controlling Uniformity of Photopolymerized Microscopic Hydrogels. *Lab Chip* **2014**, *14* (9), 1551–1563.

(36) Filatov, N. A.; Nozdriukhin, D. V.; Bukatin, A. S. The Kinetic Study of

Solidification PEGDA Microparticles in Flow-Focusing Microfluidic Chip. *J. Phys. Conf. Ser.* **2017**, *917* (4), 1–5.

(37) Chen, J.; Huang, K.; Chen, Q.; Deng, C.; Zhang, J.; Zhong, Z. Tailor-Making Fluorescent Hyaluronic Acid Microgels via Combining Microfluidics and Photoclick Chemistry for Sustained and Localized Delivery of Herceptin in Tumors. *ACS Appl. Mater. Interfaces* **2018**, *10* (4), 3929–3937.

(38) Jeong, W. C.; Kim, S. H.; Yang, S. M. Photothermal Control of Membrane Permeability of Microcapsules for On-Demand Release. *ACS Appl. Mater. Interfaces* **2014**, *6* (2), 826–832.

(39) Homayun, B.; Sun, C.; Kumar, A.; Montemagno, C.; Choi, H. J. Facile Fabrication of Microparticles with PH-Responsive Macropores for Small Intestine Targeted Drug Formulation. *Eur. J. Pharm. Biopharm.* **2018**, *128* (March), 316–326.

(40) Huang, S.; Lin, B.; Qin, J. Microfluidic Synthesis of Tunable Poly-(N-Isopropylacrylamide) Microparticles via PEG Adjustment. *Electrophoresis* **2011**, *32* (23), 3364–3370.

(41) Zhang, K.; Wu, W.; Guo, K.; Chen, J.; Zhang, P. Synthesis of Temperature-Responsive Poly(N-Isopropyl Acrylamide)/ Poly(Methyl Methacrvlate)/Silica Hybrid Capsules from Inverse Pickering Emulsion Polymerization and Their Application in Controlled Drug Release. *Langmuir* **2010**, *26* (11), 7971–7980.

(42) Budhlall, B. M.; Marquez, M.; Velev, O. D. Microwave, Photo- And Thermally Responsive PNIPAm-Gold Nanoparticle Microgels. *Langmuir* **2008**, *24* (20), 11959–11966.

(43) Heida, T.; Neubauer, J. W.; Seuss, M.; Hauck, N.; Thiele, J.; Fery, A. Mechanically Defined Microgels by Droplet Microfluidics. *Macromol. Chem.*

*Phys.* **2017**, *218* (2), 1–19.

(44) Ekici, S.; Ilgin, P.; Yilmaz, S.; Aktas, N.; Sahiner, N. Temperature and Magnetic Field Responsive Hyaluronic Acid Particles with Tunable Physical and Chemical Properties. *Appl. Surf. Sci.* **2011**, *257* (7), 2669–2676.

(45) Seiffert, S.; Thiele, J.; Abate, A. R.; Weitz, D. A. Smart Microgel Capsules from Macromolecular Precursors. **2010**, *01238* (14), 1–9.

(46) Akbari, S.; Pirbodaghi, T.; Kamm, R. D.; Hammond, P. T. A Versatile Microfluidic Device for High Throughput Production of Microparticles and Cell Microencapsulation. *Lab Chip* **2017**, *17* (12), 2067–2075.

(47) Steinhilber, D.; Rossow, T.; Wedepohl, S.; Paulus, F.; Seiffert, S.; Haag, R. A Microgel Construction Kit for Bioorthogonal Encapsulation and PH-Controlled Release of Living Cells. *Angew. Chemie - Int. Ed.* **2013**, *52* (51), 13538–13543.

(48) Celetti, G.; Natale, C. Di; Causa, F.; Battista, E.; Netti, P. A. Functionalized Poly(Ethylene Glycol) Diacrylate Microgels by Microfluidics: In Situ Peptide Encapsulation for in Serum Selective Protein Detection. *Colloids Surfaces B Biointerfaces* **2016**, *145*, 21–29.

(49) Wang, W.; Liu, L.; Ju, X. J.; Zerrouki, D.; Xie, R.; Yang, L.; Chu, L. Y. A Novel Thermo-Induced Self-Bursting Microcapsule with Magnetictargeting Property. *ChemPhysChem* **2009**, *10* (14), 2405–2409.

(50) Wang, J.; Zhu, X.; Wei, L.; Ye, Y.; Liu, Y.; Li, J.; Mei, T.; Wang, X.; Wang, L. Controlled Shape Transformation and Loading Release of Smart Hemispherical Hybrid Microgels Triggered by 'Inner Engines.' *ChemistrySelect* **2018**, *3* (15), 4067–4074.

(51) Kim, B.; Soo Lee, H.; Kim, J.; Kim, S. H. Microfluidic Fabrication of Photo-Responsive Hydrogel Capsules. *Chem. Commun.* **2013**, *49* (18), 1865–1867.

(52) Gomez, L.; Sebastian, V.; Irusta, S.; Ibarra, A.; Arruebo, M.; Santamaria, J. Scaled-up Production of Plasmonic Nanoparticles Using Microfluidics: From Metal Precursors to Functionalized and Sterilized Nanoparticles. *Lab Chip* **2014**, *14* (2), 325–332.

(53) Preciado-Flores, S.; Wang, D.; Wheeler, D. A.; Newhouse, R.; Hensel, J. K.; Schwartzberg, A.; Wang, L.; Zhu, J.; Barboza-Flores, M.; Zhang, J. Z. Highly Reproducible Synthesis of Hollow Gold Nanospheres with near Infrared Surface Plasmon Absorption Using PVP as Stabilizing Agent. *J. Mater. Chem.* **2011**, *21* (7), 2344–2350.

(54) Choi, C.-H.; Jung, J.-H.; Kim, D.-W.; Chung, Y.-M.; Lee, C.-S. Novel One-Pot Route to Monodisperse Thermosensitive Hollow Microcapsules in a Microfluidic System. *Lab Chip* **2008**, *8* (9), 1544.

(55) Gu, H.; Duits, M. H. G.; Mugele, F. Droplets Formation and Merging in Two-Phase Flow Microfluidics. *Int. J. Mol. Sci.* **2011**, *12* (4), 2572–2597.

(56) Nguyen, N.-T.; Wereley, S. T.; Shaegh, S. A. M. *Fundamentals and Applications of Microfluidics*, Third Edit.; 2019.

(57) Khan, I. U.; Stolch, L.; Serra, C. A.; Anton, N.; Akasov, R.; Vandamme, T. F. Microfluidic Conceived PH Sensitive Core-Shell Particles for Dual Drug Delivery. *Int. J. Pharm.* **2015**, *478* (1), 78–87.

(58) Carter, S.; Hunt, B.; Rimmer, S. Highly Branched Poly(N-Isopropylacrylamide)s with Imidazole End Groups Prepared by Radical Polymerization in the Presence of a Styryl Monomer Containing a Dithioester Group. *Macromolecules* **2005**, *38* (11), 4595–4603.

(59) Rimmer, S.; Carter, S.; Rutkaite, R.; Haycock, J. W.; Swanson, L. Highly Branched Poly-(N-Isopropylacrylamide)s with Arginine-Glycine- Aspartic Acid

(RGD)- or COOH-Chain Ends That Form Sub-Micron Stimulus-Responsive Particles above the Critical Solution Temperature. *Soft Matter* **2007**, *3* (8), 971–973.

(60) Feil, H.; Bae, Y. H.; Feijen, J.; Kim, S. W. Effect of Comonomer Hydrophilicity and Ionization on the Lower Critical Solution Temperature of N-Isopropylacrylamide Copolymers. *Macromolecules* **1993**, *26* (10), 2496–2500.

(61) Yang, Y. J.; Tang, B.; Zhang, L.; Wang, C.; Ma, H. T.; Pang, D. W.; Zhang, Z. L. On-Demand One-Step Synthesis of Small-Sized Fluorescent-Magnetic Bifunctional Microparticles on a Droplet-Splitting Chip. *J. Mater. Chem. B* **2018**, *6* (6), 961–965.

(62) ISO 10993-5:2009 - Biological Evaluation of Medical Devices – Part 5: Tests for in Vitro Cytotoxicity. Http://Www.Iso.Org/Iso/Catalogue_detail.Htm?Csnumber=36406.